Biochemically altered myelin triggers autoimmune demyelination

Andrew V. Caprariello[a], James A. Rogers[a], Megan L. Morgan[a], Vahid Hoghooghi[a], Jason R. Plemel[a], Adam Koebel[b,c], Shigeki Tsutsui[a], Jeffrey F. Dunn[a], Lakshmi P. Kotra[b,c], Shalina S. Ousman[a], V. Wee Yong[a], and Peter K. Stys[a,1]

[a]Department of Clinical Neurosciences, Hotchkiss Brain Institute, University of Calgary Cumming School of Medicine, Calgary, AB T2N 4N1, Canada; [b]Center for Molecular Design and Preformulations, Toronto General Hospital Research Institute, University of Toronto, Toronto, ON, M5G 2C4 Canada; and [c]Department of Pharmaceutical Sciences, Leslie Dan Faculty of Pharmacy, University of Toronto, Toronto, ON, M5G 2C4 Canada

Although immune attack against central nervous system (CNS) myelin is a central feature of multiple sclerosis (MS), its root cause is unresolved. In this report, we provide direct evidence that subtle biochemical modifications to brain myelin elicit pathological immune responses with radiological and histological properties similar to MS lesions. A subtle myelinopathy induced by abbreviated cuprizone treatment, coupled with subsequent immune stimulation, resulted in lesions of inflammatory demyelination. The degree of myelin injury dictated the resulting immune response; biochemical damage that was too limited or too extensive failed to trigger overt pathology. An inhibitor of peptidyl arginine deiminases (PADs), enzymes that alter myelin structure and correlate with MS lesion severity, mitigated pathology even when administered only during the myelin-altering phase. Moreover, cultured splenocytes were reactive against donor myelin isolates, a response that was substantially muted when splenocytes were exposed to myelin from donors treated with PAD inhibitors. By showing that a primary biochemical myelinopathy can trigger secondary pathological inflammation, "cuprizone autoimmune encephalitis" potentially reconciles conflicting theories about MS pathogenesis and provides a strong rationale for investigating myelin as a primary target for early, preventative therapy.

multiple sclerosis | immunopathogenesis | citrullination | myelin | cuprizone

Despite progress in understanding the pathobiology of multiple sclerosis (MS) (1, 2), its root cause remains unknown. Conventional views hold that dysregulated immune attacks against myelin, a fatty substance which ensheathes and supports axons in the central nervous system (CNS), cause the characteristic focal lesions of inflammatory demyelination. However, neither the immune triggers nor their targets have been identified, and despite potent immune-modulating therapies, for most patients the progression to disability remains inevitable. Given these limitations, the notion that unchecked immune attacks on myelin from the "outside in" has been countered by the argument that pathology of CNS myelin precedes and triggers inflammatory demyelination from the "inside out" (3). We hypothesize that the characteristic T2-hyperintense MS lesions reflect but the tip of a pathological iceberg, i.e., the later manifestation of an insidious precursory myelinopathy with secondary autoimmunity. Consistent with this notion, a MS prodrome was recently described (4) and later supported by findings of brain abnormalities in at-risk but asymptomatic individuals (5). Together, these results suggest a window of opportunity for early preventative therapies that target the earliest pathological events in the MS brain. Proof of principle in an animal model that a subtle myelinopathy triggers autoimmune inflammation—and therefore represents a proximal driver of inflammatory demyelination—would represent a major advance in the field.

Biochemically altered myelin—in particular, deimination of myelin basic protein, a major myelin constituent that influences its compaction—is one such brain-localized event previously implicated in the development of autoimmunity (6). The extent of modified myelin biochemistry correlates with the severity of MS lesion subsets (7–9); yet suitable animal models in which to dissect cause from effect are lacking (10, 11). The death of myelin-forming oligodendroglial cells—present in a subset of MS lesions (12, 13)—could also initiate autoimmunity, but initial experiments to test this theory directly were negative (14). However, subsequent studies injected new life into the debate. First, Traka et al. (15) demonstrated that oligodendrocyte-induced immune autoreactivity does occur but only a full year after cell death. Important corroboration followed showing that brain-intrinsic degenerative cascades induce immune infiltration and destruction (16, 17). These collective advances notwithstanding, the precise CNS targets of an unchecked immune system, including myelin itself, remain unsettled. Experimental autoimmune encephalomyelitis (EAE), a widely used model of MS, has provided important clues (18). Although EAE clearly demonstrates the destructive potential of immune cells primed by peripheral injection of extrinsic myelin proteins, it necessarily precludes the identification of intrinsic upstream inflammatory triggers. Autoimmunity elicited by endogenous, in vivo-generated myelin proteins or lipids would facilitate studies focused on mechanisms of myelin-induced autoimmunity and its contributions to MS pathology.

The links between altered myelin biochemistry and pathological demyelination are becoming increasingly clear. Recent studies, for example, have implicated structural changes in myelin membranes (11), particularly myelin basic protein (10), as initiators of myelin

Significance

Caprariello et al. demonstrate that subtle biochemical pathology to axon-ensheathing myelin, in the absence of overt demyelination, is sufficient to elicit severe secondary demyelinating inflammatory reactions. The resulting lesions bear radiological and histological resemblance to inflammatory demyelinating lesions of multiple sclerosis (MS), raising the possibility that subtle myelin degeneration in the MS brain may be a proximal event in the evolution of inflammation and consequent myelin loss. Consistent with an "inside-out" model of MS pathogenesis, these findings provide a rationale for investigating myelin as a target for early preventive therapy.

sheath unraveling. However, direct proof that primary abnormalities of myelin secondarily drive inflammatory demyelination is lacking. Here we describe a unique mouse model, cuprizone autoimmune encephalitis (CAE), that illuminates mechanisms through which biochemically destabilized myelin triggers a pathological demyelinating immune response comparable to active MS plaques. CAE identifies primary myelin pathology in an immune-predisposed host as a potent trigger of inflammatory demyelination. In so doing, the model emphasizes pathological myelin, particularly its citrullinated form, as a target for new therapies in all stages of MS.

Results

Subtle Myelinopathy Triggers Inflammatory Demyelination in Immune-Dysregulated Hosts.
To interrogate the immunogenicity of endogenously degraded myelin, we designed an animal model (Fig. 1A) to test whether biochemical myelin modifications could trigger lesions of inflammatory demyelination. Reasoning that subdemyelinating changes to CNS myelin were key to its potential immunogenicity, we first administered an abbreviated 2-wk treatment of the demyelinating compound cuprizone (CPZ), a period sufficiently brief so as to perturb myelin ultrastructure without causing overt demyelination (Fig. 1B). Such an abbreviated CPZ "induction phase" was then followed by an artificial immune boost (IB) of complete Freund's adjuvant and pertussis toxin (PTx), an immune stimulus routinely used in EAE. Unlike EAE, critically, exogenous myelin peptides were deliberately excluded from the adjuvant in our experiments so that the immunogenicity of endogenous, CPZ-altered myelin (19) could be directly tested. Two weeks of CPZ and then IB were followed by a 2-wk incubation phase to allow time for a potential immune response to be mounted and for immunosuppressive effects of CPZ (20, 21) to dissipate. As a noninvasive surrogate marker of inflammation, gadolinium (Gd)-contrast qT1 MRI sequences were acquired halfway into the 2-wk incubation phase (Fig. 1C). Additional MRI imaging was performed at various times during the study to complement standard histological and biochemical analysis.

One week after IB, there was minimal Gd enhancement in three separate control groups: naive untreated, IB only (i.e., no CPZ), and CPZ only (i.e., no IB). By contrast, the combination of abbreviated, 2-wk CPZ then IB resulted in brains that were strongly Gd enhancing, indicating a breakdown of the blood–brain barrier, a feature associated with the pathological infiltration of immune cells. Periventricular enhancement suggested a possible breach also of the barrier separating the brain from the cerebrospinal fluid. In addition to periventricular enhancement, white matter tracts such as corpus callosum also exhibited significant enhancement ("CPZ then IB"; Fig. 1 C and E). Two weeks after abbreviated CPZ without intervening IB ("CPZ no IB"), radiological and histological abnormalities were absent in 20 of the 24 control animals examined (Fig. 1D); the four outlier controls were inflamed and demyelinated, but interestingly at the time of harvest, two of the four had severe traumatic fight wounds and therefore likely elevated systemic inflammation. Since the effects of CPZ are delayed, myelin was examined 3 wk after an abbreviated, 2-wk CPZ course (without IB); no significant demyelination (SI Appendix, Fig. S1A) nor inflammatory hypercellularity were detected (SI Appendix, Fig. S1). In striking contrast, a combination of abbreviated CPZ followed by IB resulted in white matter T2 hyperintensites in all 24 animals. In the worst cases, significant radiological abnormalities spanned nearly 60% of the anterior–posterior extent of the corpus callosum (Fig. 1F). Standard myelin histopathology revealed overt demyelination and dense infiltration of neutral red-positive cells in the splenium of the corpus callosum (Fig. 1D, far Right Inset). Taken together, only the combination of abbreviated CPZ together with IB resulted in severe inflammatory demyelination.

Extent of Myelin Modification Modulates the Resulting Immune Response.
To examine whether the degree of myelin pathology influenced the resulting inflammatory responses, separate cohorts were exposed
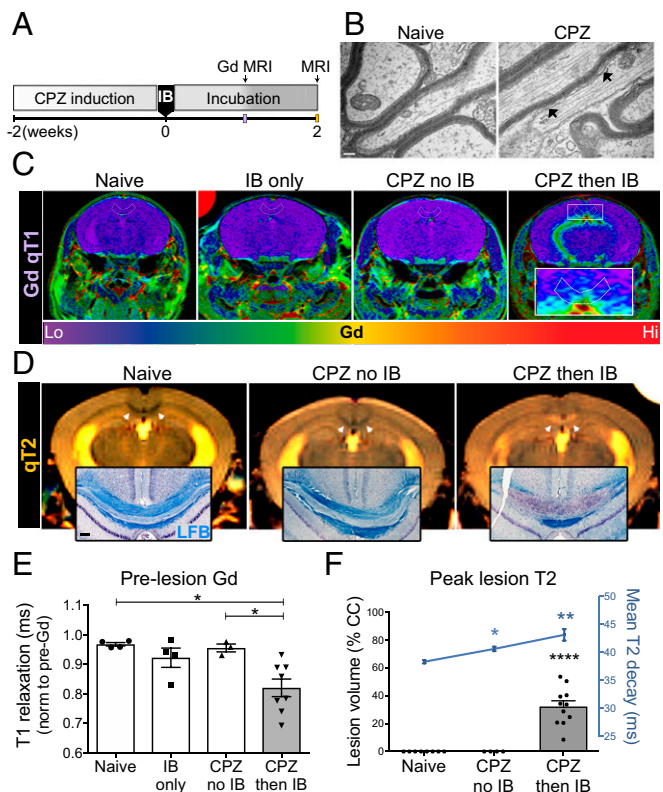

Fig. 1. Subdemyelinating cuprizone (CPZ) triggered Gd-enhancing lesions of inflammatory demyelination. (A) Brief CPZ in an induction phase was followed by immune boost (IB) and a 2-wk incubation period on regular chow. (B) Electron micrographs of myelin ultrastructure indicate that CPZ exposure was sufficiently brief as to alter but largely preserve myelin. (C) One-week post-IB, compared with naive, IB only, or CPZ only, only the combination of abbreviated CPZ then IB resulted in significant Gd enhancement (orange/red). (D) Two-weeks post-IB, compared with controls, CPZ+IB brains alone exhibited obvious T2 white matter lesions (white arrowheads; increased signal intensity on MRI) that corresponded to inflammatory demyelination, a reaction that was termed cuprizone autoimmune encephalitis (CAE). (E) Quantification of T1 relaxation-shortening effects of brain Gd, indicative of inflammation and blood–brain barrier leakage, were observed only in CPZ+IB. (F) T2w MRI reflected the severity and extent of CAE lesions, with cases that involved nearly 60% of the anterior–posterior extent of the corpus callosum. Each data point is an individual subject and bars represent SEM. EM, $n = 6$; Gd MRI, $n = 4$ naive; $n = 6$ IB only; $n = 3$ CPZ only; $n = 8$ CPZ then IB. Histology, $n = 12$ naive controls; $n = 13$ IB only; $n = 24$ CPZ only; $n = 24$ CPZ then IB. Significance was determined by one-way ANOVA. *$P < 0.05$, **$P < 0.01$, ****$P < 0.0001$. (Scale bars: B, 100 nm; D, Insets, 100 μm.)

to shorter or longer CPZ inductions (Fig. 2A). The subsequent IB plus 2-wk incubation period depicted in Fig. 1A remained unchanged. If myelin injury were the driving force for a pathological immune response, then a shorter, 1-wk CPZ induction paradigm might not trigger inflammatory demyelination. Indeed, similar to IB-only controls (0+IB+1), there was no significant Gd enhancement in the 1-wk CPZ induction group (1+IB+1; Fig. 2 B and C). If presence of particular myelin antigens was necessary for the pathological inflammation, then a longer 3-wk CPZ induction phase, sufficient to cause noninflammatory demyelination (22), might also fail to trigger an inflammatory response due to debris clearance. In contrast to strong Gd enhancement following a 2-wk CPZ induction (2+IB+1; Fig. 2D), a 3-wk induction (3+IB+1) generated minimal Gd enhancement (Fig. 2E). In all induction paradigms, brains were harvested 2 wk after IB for histopathological analysis. In IB-only controls, immune activity was relatively quiescent as indicated by immunostaining with CD45 and Iba1, and
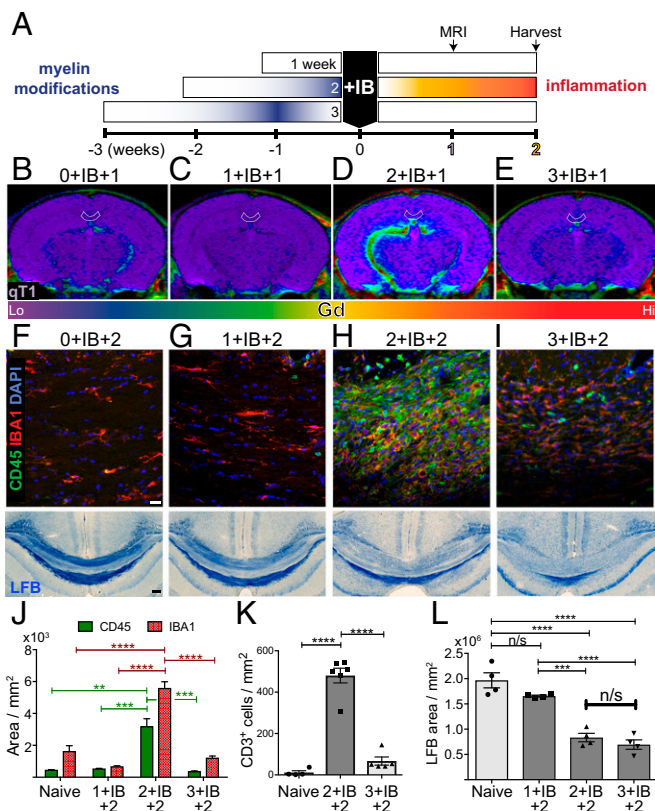
Fig. 2. The extent of myelin modifications modulated the resulting immune response. (*A*) Shorter or longer CPZ induction paradigms (1 and 3 wk) were followed, as in Fig. 1, by IB and a 2-wk incubation period. (*B*) Compared with IB alone, neither shorter (*C*) nor longer (*E*) CPZ induction periods resulted in significant Gd enhancement compared with an induction of 2 wk (*D*), previously shown to trigger inflammatory demyelination. At 2-wk post-IB, histopathology showed minimal inflammation in tissue sections from all conditions except those treated with 2 wk of CPZ followed by IB and 2 wk of incubation (2+IB+2; *H*). Namely, IB only (0+IB+2; *F*), 1-wk CPZ induction (1+IB+2; *G*), and 3-wk CPZ induction (3+IB+2; *I*) all contained significantly fewer CD45^{+} and Iba1^{+} cells. Inflammatory responses correlated with degree of LFB myelin loss (blue). The lone exception was the 3+IB+2 group, which was demyelinated as expected but not inflamed. (*L*) Noninflammatory myelin loss in 3+IB+2 was matched by inflammatory demyelination in 2+IB+2. [Scale bars: *F*, *Upper*, 10 μm; *Lower*, 100 μm (also apply to *G*–*I*).] Error bars represent SEM. Every data point in *K* and *L* is a distinct subject. $n = 4$–6 for all groups. Significance was determined by one-way ANOVA. **$P < 0.01$, ***$P < 0.001$, ****$P < 0.0001$; n/s, not significant.

myelin remained fully intact (Fig. 2*F*). A similar immune quiescence was observed in the 1-wk CPZ induction group (Fig. 2*G*) where, in striking contrast to 2-wk CPZ induction (Fig. 2*H*), neither demyelination, microglial activation, nor leukocyte infiltration were apparent. Three weeks of CPZ+IB, showing predictable demyelination, did not promote significant cellular infiltration after IB (Fig. 2*I*); in fact, after 3-wk CPZ, IB altered neither the extent of demyelination nor the amount of cellular infiltration (*SI Appendix*, Fig. S3). These results demonstrate that not only the extent of myelin pathology but also its sustained presence profoundly influenced subsequent inflammatory responses (Fig. 2 *J* and *K*). Importantly, the extent and timing of myelin alteration/clearance critically determined the extent of demyelination (Fig. 2*L*). We concluded that an optimal state of biochemical myelin modification was required to elicit secondary inflammatory demyelination: very short CPZ exposure before IB likely generated insufficient myelin immunogens, whereas more prolonged treatment resulted in excessive demyelination and clearance of immunogenic myelin debris. Having established the optimal induction phase to be 2 wk

of CPZ, the remainder of the experiments were conducted using this paradigm, and hereafter will be referred to as CAE.

To identify the infiltrating cells within CAE lesions, we probed tissue sections with cell-specific antibodies. CD3^{+} T cells infiltrated CAE brains, unlike either IB-only or CPZ-only controls (*SI Appendix*, Fig. S2 *A* and *A′*). Adjacent sections of the lesions colabeled with panleukocyte CD45 and the microglia/macrophage marker Iba1 indicated a significant leukocyte accumulation as well as a marked increase in Iba1 fluorescence (*SI Appendix*, Fig. S2 *B* and *B′*). Substantial astrogliosis was also evident by significantly increased GFAP[+] immunoreactivity within CAE lesions (*SI Appendix*, Fig. S2 *C* and *C′*). Axonal integrity, assessed by quantification of panneurofilament labeling, indicated significant axonal dropout only in the CAE group (*SI Appendix*, Fig. S2 *D* and *D′*). To verify the peripheral origins of a subset of the infiltrated monocyte/macrophage populations, parallel experiments were conducted in double transgenic mice in which a promoter specific to macrophages/microglia, CX3CR1-Cre[ER], was crossed with Ai9 [Rosa-CAG-floxSTOP–TdT (tomato red fluorescence protein reporter)]. The differential capacity for self-renewal in central versus peripheral monocytes/macrophages allowed binary discrimination on the basis of sustained TdT fluorescence in cells colabeled with Iba1. Only in CAE groups were there Iba1^{+} cells lacking a TdT reporter (*SI Appendix*, Fig. S2 *E* and *E′*) suggestive of peripheral macrophages/monocytes. Thus, demyelination in CAE lesions was accompanied by myriad histopathologies resembling active MS lesions, including Gd enhancement, T-cell infiltration, elevated innate immunity, astrogliosis, and axonal loss.

Citrullination Links Myelinopathy and Pathological Inflammation in CAE. We next sought to define molecular mechanisms by which biochemically altered myelin drives inflammatory demyelination. Peptidyl arginine deiminases (PADs), a family of enzymes known to biochemically alter and destabilize myelin in immune-stimulating ways (6, 8, 23), are strongly up-regulated in subsets of MS lesions (7). To examine whether PADs also underlie CAE, a small molecule PAD inhibitor, KP-302, (compound 23 in ref. 24) was administered intraperitoneally (50 mg/kg) once daily during both the induction and incubation phases. KP-302 conferred highly significant protection from inflammatory demyelination (Fig. 3 *A* and *B*). To exclude antiinflammatory effects of KP-302, the compound was administered either during the CPZ induction phase only (Fig. 3*C*) or the post-IB incubation phase only (*SI Appendix*, Fig. S5). Inflammatory demyelination was reduced only when KP-302 was administered during the induction but not the incubation phase. Furthermore, Western blots indicated that citrullination, as a function of CPZ exposure during the induction phase, peaked at the 2-wk period when IB had the greatest effect. Increased citrullination at molecular weights corresponding to MBP isoforms was consistent with deimination of the many arginine residues present on this predominant myelin protein (Fig. 3*F* and *SI Appendix*, Fig. S4). Finally, immunohistochemistry revealed increases in both citrulline and decompacted myelin (QD9) in affected white matter regions of CAE animals (Fig. 3 *G*–*I*). Taken together, these data implicate citrullinated proteins, likely those of CPZ-altered myelin, as the primary drivers of CAE lesions.

CAE Splenocytes React Specifically to Citrullinated Myelin. To test whether CAE splenocytes were reacting specifically to citrullinated myelin, antigen recall experiments were carried out. Splenocytes from CAE animals at the peak of inflammatory demyelination (i.e., the 2+IB+2 time point) were cultured and exposed to either naive myelin or that of varying states of citrullination isolated from donor mouse brains by gradient ultracentrifugation (25). Specific lock-and-key interactions between splenocytes and donor CPZ myelin were demonstrated by significant and specific increases in cell proliferation after 72 h of stimulation (Fig. 4*A*). Consistent with autoreactivity to citrullinated
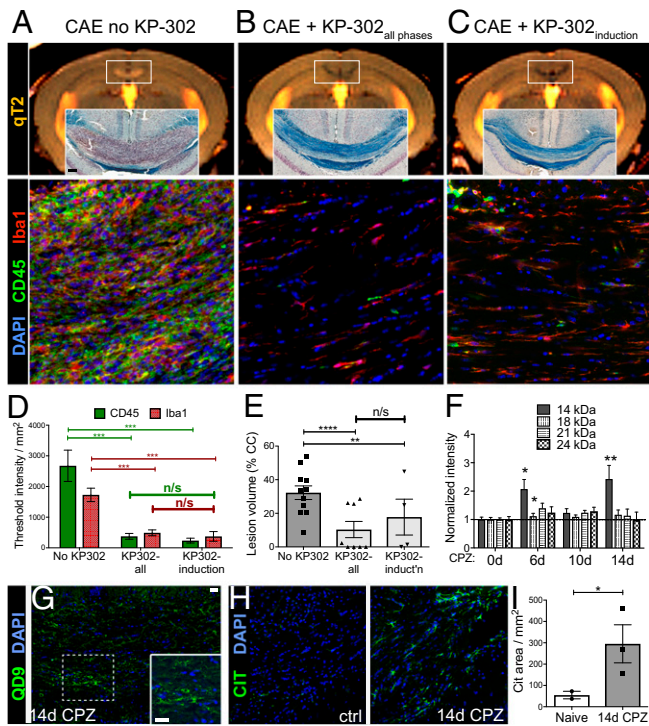
Fig. 3. Myelin citrullination was a major driver of CAE. (*A*) Without the small molecule PAD inhibitor KP-302, white matter T2 lesions (bright orange in top white box) in CAE (2+IB+2) brains were accompanied by inflammation and demyelination (*Inset*, blue/purple), and elevated CD45 and Iba1 fluorescence (green/red). (*B*) By contrast, KP-302 (50 mg/kg intraperitoneally, once daily) during both induction and incubation phases strongly mitigated myelin loss and reduced inflammation. (*C*) When administered during only the CPZ-induction phase, KP-302 was as effective as when delivered throughout both phases, reducing CD45/Iba1 immunofluorescence (*D*) and decreasing radiological lesion burden (*E*), in contrast to minimal protection afforded by the drug given postinduction only (*SI Appendix*, Fig. S5). (*F*) Western blot for citrullinated proteins at the end of the CPZ-induction phase demonstrated an upregulation of citrullines particularly at MBP-relevant molecular weights. (*G* and *H*) Immunostaining showed degenerated myelin (QD9 in *G*) and increased citrullination (*H* and *I*) within callosal regions vulnerable to CAE. Error bars represent SEM. For each time point in *F*, $n = 5$ (*SI Appendix*, Fig. S4). Significance was determined by one-way ANOVA. *$P < 0.05$, **$P < 0.01$, ***$P < 0.001$, ****$P < 0.0001$; n/s, not significant. [Scale bars: *A, Upper Insets*, 100 μm; *A, Lower* 10 μm (scale bars in *A* also apply to *B* and *C*); *G* and *G, Inset*, 20 μm (scale bar in *G* also applies to *H*).]

myelin, myelin derived from CPZ animals treated with KP-302 to prevent in vivo citrullination did not activate the cultured cells (Fig. 4*B*). Although naive myelin also stimulated CAE splenocytes, this response was abrogated by in vivo treatment with KP-302, suggesting a high degree of sensitivity of CAE splenocytes to even low levels of physiological citrullination. Furthermore, the strength of the splenocyte response correlated with the degree of citrullination induced by varying durations of CPZ treatment (Fig. 4*C* and *SI Appendix*, Fig. S4). Taken together, the myelin specificity of CAE splenocytes combined with the muted reaction to myelin from KP-302–treated animals suggested that inflammatory demyelination in CAE reflected biochemically modified myelin driving a potent, secondary autoimmune response that was dependent on PAD-mediated, citrullinated, endogenous peptides.

Discussion

Our CAE model provides clear proof of principle that subtle myelinopathy can trigger inflammatory demyelination, a concept that carries important implications for MS pathogenesis. CAE posits a working model of MS in which subclinical myelin perturbations

accruing during an early prodromal or induction phase, convert underlying immune susceptibilities (26, 27) into self-myelin autoimmune attacks. Such a mechanism could elegantly reconcile current conflicting theories of MS lesion development: autoimmune myelin destruction from the outside in may be the most obvious pathological manifestation of subclinical myelin pathology that, from the inside out (3), ultimately predisposes the patient to accelerated inflammatory destruction. Unremitting biochemical myelin alterations, ongoing from the earliest stages of MS, could explain why even potent immune-modulating therapies fail to halt later-stage MS progression and ensuing disability; once autoimmune inflammation largely subsides, either with immune-modulating therapy or with age by immune senescence, the underlying progressive biochemical pathology of myelin continues unabated, leading to degeneration of axoglial elements and irreversible disability.

Although our data clearly demonstrate a causal link between myelin modifications and inflammatory demyelination in mouse, this link remains unresolved in humans. Nevertheless, evidence is mounting that even very early phases of MS harbor significant pathological changes (28, 29). Indeed, a recent report of radiological brain abnormalities in asymptomatic yet at-risk individuals (5) raises the possibility that underestimated, as yet unidentified, CNS pathologies exist early in the disease process. Furthermore, a longitudinal analysis of dysregulated proteins in pediatric MS implies that perturbed axoglial physiology may be a feature of the earliest events
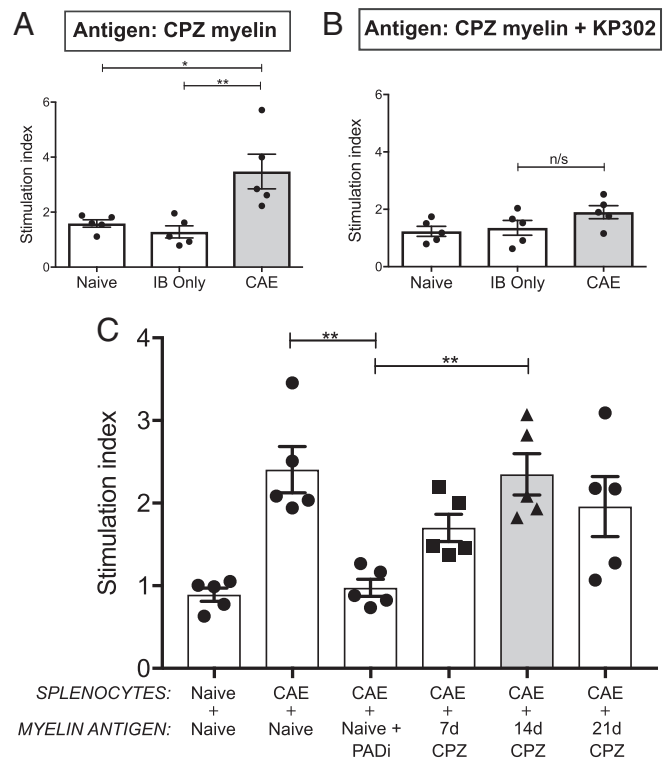

Fig. 4. CAE splenocytes reacted robustly and specifically to donor myelin. (*A*) Relative to splenocytes from naive controls without added antigens, cells derived from animals at the peak of CAE proliferated in response to myelin isolated from donor CPZ mouse brains. (*B*) CAE splenocytes were unreactive to myelin derived from CPZ animals treated in vivo with KP-302. (*C*) CAE splenocytes also reacted to naive myelin but not when the same naive donors were treated in vivo with KP-302. The duration of CPZ treatment—tied to varying degrees of citrullination (*SI Appendix*, Fig. S4)—modulated the resulting responses of CAE splenocytes. Each dot represents the mean of three technical antigen replicates from a single mouse in which $n = 5$ mice for all splenocyte sources and $n = 3$–4 mice for myelin isolates. Significance was determined by one-way ANOVA. *$P < 0.05$, **$P < 0.01$; n/s, not significant.

IMMUNOLOGY AND INFLAMMATION

of MS pathogenesis (30), although the initiating sites and molecules involved remain unresolved. The identification in CAE of citrullinated myelin as a CNS-localized trigger of focal inflammatory demyelination, a molecular pathway previously linked to both autoimmunity and MS severity, demonstrates the utility of our model for unraveling mechanisms of myelin-induced autoimmunity.

The role of ultrastructural myelin changes identified in early MS lesions for disease pathogenesis has yet to be clarified. Electron micrographs of acute MS lesions reveal conspicuous pathology at the inner tongue of myelin (31–33), the significance of which has since been corroborated experimentally in models spanning primary autoimmunity (10) to those chiefly of non-immune demyelination (34). However, no single animal model has been able to demonstrate inflammatory demyelination caused by endogenous, in vivo-generated myelin debris, that we argue could underpin MS pathogenesis. PAD-modified myelin, present in MS lesions and directly correlated with disease severity (7), is less stable and more immunogenic (35). Hypercitrullination of MBP strongly correlates with sites of lymphocyte infiltration and destruction in EAE (36), further underscoring the immunogenic nature of deiminated myelin proteins. However, precisely how citrullinated myelin is immunogenic is unclear. The response of CAE splenocytes to myelin isolated from naive controls argues that all myelin, by virtue of its baseline citrullination, may be antigenic, and perhaps a threshold of citrullination exists above which pathological immune responses occur. Myelin citrullination, together with resultant decompaction, likely conspire to generate an antigenic milieu accessible to immune effectors. Intriguing increases in PAD activity have been shown in normal-appearing MS white matter (9, 37), which together with our findings, argues further for a direct causative role of myelin hypercitrullination in the genesis of inflammatory lesions, both in our CAE model, and in MS (Fig. 5).

Our data taken together with previous observations from human MS are consistent with an early, subclinical "biochemical dysmyelination" as the proximal event that drives both autoimmune inflammatory MS pathology and a parallel cytodegenerative process that continues during and after the inflammatory phase of clinical MS. Predicated on endogenous myelin antigens driving a secondary immune response, CAE opens potential new avenues of investigation into the underlying pathobiology of this disease, and represents an attractive preclinical model for testing novel therapeutics aimed at both degenerative and inflammatory processes, that in combination may be most effective for all phases of MS.

Materials and Methods

CAE Induction. Male C57BL/6 mice (Charles River), 7–8 wk of age, were fed ad libitum CPZ (0.2% wt/wt) crushed up in standard rodent chow for 2 wk. On the day of CPZ cessation, under isoflurane anesthesia, complete Freund's adjuvant (11 mg/mL *Mycobacterium tuberculosis*) was s.c. and bilaterally injected in the hindlimbs as per standard EAE protocols, except for the addition of myelin or any other additional peptides. PTx (0.015 mg/kg) was then intraperitoneally injected. Two days later, an equivalent second dose of PTx was administered. All experiments involving small molecule PAD inhibitors (KP-302) involved i.p. dosing (50 mg/kg) once daily. Refer to ref. 24 for detailed synthesis, chemical procedure, and characterization data for KP-302.

MRI Sequences. Animals were imaged in a 9.4T Bruker MRI scanner with an Avance console and Paravision 5.1 while stabilized under isoflurane anesthesia in a small rodent, 35-mm volume coil with the following sequences: for qT2, a multiecho Carr–Purcell–Meiboom–Gill sequence was acquired [first echo 6 ms, interecho spacing 6 ms, 128 echoes, repetition time (TR) = 3,000 ms, 1.92 cm field of view (FOV), 1-mm slice, matrix = 128 × 128, 4 averages]; in the same imaging session as CPMG, an anatomical T2w image was also collected by fast spin echo [echo time (TE) = 32 ms, rare factor = 8, TR = 4,000 ms, 2 cm FOV, 0.5-mm slice thickness, 25 slices, matrix = 256 × 256, 1 average]. Voxel-wise mean T2 decay times were calculated, data for regions of interest were averaged to a single value, and group differences were assessed by one-way ANOVA. For Gd imaging, first a pre-Gd qT1 was acquired using a fast spin echo variable TR (VTR) sequence (TR = 250, 500, 1,000, 3,000, 7,500 ms, TE = 20 ms, rare factor = 4, 2 cm FOV, 5 slices, 0.5 mm/slice, 256 × 128, 2 averages).
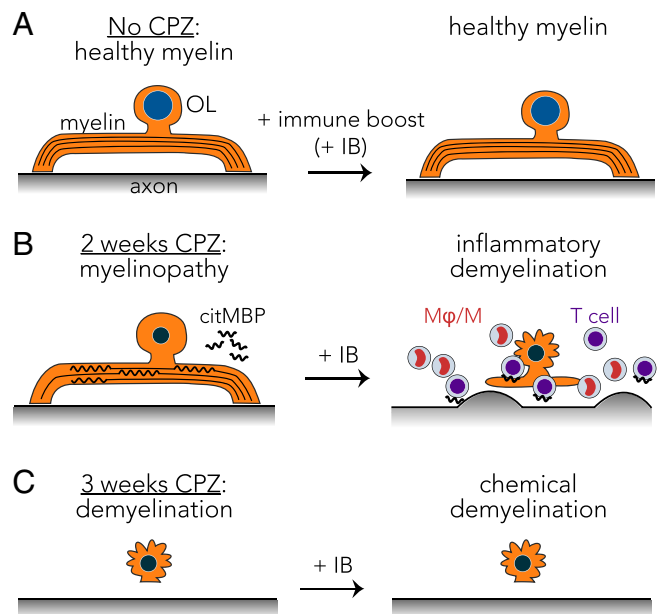
Fig. 5. CAE elucidates a molecular pathway through which biochemically altered myelin triggers autoimmune demyelination in mouse. (*A*) With intact myelin, immune boost (IB) alone had little effect. (*B*) In stark contrast, an abbreviated, subdemyelinating cuprizone (CPZ) treatment induced a subtle biochemical myelinopathy [likely including citrullinated MBP (citMBP)] that, when followed by IB, secondarily triggered severe inflammatory demyelination. Such lesions are populated by citrullinated myelin-reactive innate [macrophages/microglia (Mφ/M)] and adaptive (T lymphocytes) immune cells, that drive severe demyelination and secondary and bystander axonal degeneration. (*C*) Paradoxically, IB administered after an overtly demyelinating 3-wk course of CPZ, with associated clearance of myelin antigens, had no effect. Only the combination of subtle biochemical myelin pathology together with appropriately timed immune stimulation, triggered brisk inflammatory demyelinating lesions similar to those found in MS.

After the initial pre-Gd qT1 sequence, the animal was removed from the magnet bore but not the coil so that 1 mmol/kg Gd (Magnevist) could be injected intraperitoneally. The animal was then reinserted and registered to prescan image, after which the same VTR sequence was repeated (~10 min after Gd injection). Mean post-Gd T1 relaxation times in the medial corpus callosum across all five slices were normalized against mean pre-Gd T1. Group differences were assessed by one-way ANOVA. Volumetric lesion analyses were calculated from multislice T1 and T2 MRI sequences. An observer blinded to group identities manually traced hyperintensities in the entire corpus callosum and calculated lesioned area as a percentage of total callosal volume.

Tissue Harvesting. Tissue was harvested either for histology or biochemistry at appropriate times after CPZ/immune boost. For histology, under heavy sodium pentobarbital anesthesia, mice were transcardially perfused, first with 12 mL at room temperature 1× PBS and then 12 mL ice-cold 4% paraformaldehyde. The tissue was postfixed in the same fixative at 4 °C overnight, after which it was cryoprotected first in 20% sucrose until the tissue sank and then 30% sucrose. Brains were embedded in OCT and rapidly frozen in dry-ice cooled isopentane. Twenty-micrometer sections were cut on a cryostat and collected on VWR Superfrost Plus Micro Slides (three sections per slide, region matched). For biochemistry, the tissue was harvested fresh under heavy anesthesia and flash frozen in a bath of isopentane and dry ice and kept at −80 °C until homogenization. Samples were homogenized on ice at 10% wt/wt in PBS on a drill press adapted for this purpose and kept at −80 °C until experimentation.

Tissue Histochemistry. Fixed, frozen tissue sections were stained with Luxol Fast Blue (LFB) (Solvent Blue 38, Sigma-Aldrich) for myelin and counterstained with Neutral Red (Avantor). Stained brain sections were imaged on a Thorlabs EnVista whole-slide scanning microscope. The area of LFB staining was calculated in ImageTrak (version 4.12.38, written by P.K.S.) by analyzing red-green-blue (RGB) components, and using blinded, manual thresholding to determine appropriate signal above noise in three sections per animal from four to six

animals per group. Mean area per square millimeter was compared between groups using one-way ANOVA.

Immunohistochemistry. The following antibodies performed optimally in unfixed frozen, 20-μm tissue sections: rabbit anti-CD3 (1:100, A0452; Dako); mouse anti-peptidyl citrulline clone F95 (MABN328, EMD Millipore). Before immunostaining, a light fixation step with 10 min ice-cold methanol was required. No antigen retrieval was necessary. Fixed, frozen 20-μm tissue sections were used for the following antibodies: rat anti-CD45 (1:100, 550539; BD Biosciences); rabbit anti-IBA1 (1:500, 019–19741; Wako); rabbit anti-GFAP (1:500, Z0334; Dako); mouse anti-panneurofilament clone SMI-312 (1:1,000, 837904; Biolegend). Mean fluorescence area per square millimeter was compared among groups using one-way ANOVA.

Western Blot. Protein concentrations of mouse brain homogenates were quantified using the Pierce BCA protein assay. Proteins were then denatured in BOLT LDS sample buffer and BOLT sample reducing agent (Novex by Life Technologies) for 10 min at 95 °C. A total of 20 μg of denatured protein per sample was resolved in BOLT 4–12% Bis-Tris Plus gels (Invitrogen) and transferred onto PVDF membranes using an iBlot 2 gel transfer device (Life Technologies). Molecular masses were estimated using Precision Plus Protein Dual Color Standards (Bio-Rad). Membranes were first incubated with membrane blocking solution (Life Technologies) for 2 h, followed by incubation with primary antibody solution (anti-peptidyl citrulline, clone F95, mouse monoclonal IGMk, EMD Millipore Corp, LOT: 2750102, 1:100 in TBST-0.1/10% BSA) for 1 h at room temperature. Membranes were then incubated for 1 h with secondary antibody solution (peroxidase-conjugated AffiniPure goat anti-mouse IgM, μ-chain specific, Jackson Immuno Research Laboratories, Inc, LOT: 124593, 1:2,000 in TBST-0.1/10% BSA). Immunochemical detection was carried out using the Novex ECL HRP chemiluminescent substrate reagent kit (Invitrogen), and imaged on a Fluor-S Max MultiImager (Bio-Rad) with Quantity One software (version 4.6.9). Signal intensities were normalized to total protein by Coomassie Blue (Brilliant Blue R, Sigma-Aldrich). Coomassie Blue-stained membranes were imaged with the ChemiDoc Touch Imaging System (Bio-Rad) and subsequent densitometry

analysis was performed in ImageJ (version 1.51f). The means of band density values were compared between experimental groups by unpaired t test.

Antigen Recall Cultures. Splenocytes were isolated from three treatment groups: naive, IB only, and CAE. Briefly, spleens were homogenized through a 70-μm cell strainer to remove spleen connective tissue. Red blood cells were lysed with 1% ammonium-chloride-potassium lysing buffer. A total of 500,000 cells per well were plated in triplicate and exposed to one of six different isolated myelin extracts (1% wt/vol) isolated from the following donor mice: naive, naive + PADi (50 mg/kg, intraperitoneal, one per day for 14 d), 1 wk of CPZ, 2 wk of CPZ, 2 wk of CPZ+PADi, and 3 wk of CPZ. To assess proliferation rates in culture, the cells were pulsed with [3H]-thymidine (1 mCi per well) after 72 h of culture and harvested 18 h later onto filter paper. The counts per minute of incorporated [3H]-thymidine were read using a beta counter.

Statistics. Statistical significance was determined using one- or two-way ANOVA with post hoc testing using either Tukey's or Sidak's tests for multiple comparisons (Prism 6.0, GraphPad software). In cases of fewer subjects, a Kruskal–Wallis test with Dunn's multiple comparisons test was utilized. All data are presented as mean ± SEM.

Study Approval. All animal experiments were carried out in accordance with protocols approved by the University of Calgary Animal Care Committee.

1. Hemmer B, Nessler S, Zhou D, Kieseier B, Hartung H-P (2006) Immunopathogenesis and immunotherapy of multiple sclerosis. *Nat Clin Pract Neurol* 2:201–211.
2. Dendrou CA, Fugger L, Friese MA (2015) Immunopathology of multiple sclerosis. *Nat Rev Immunol* 15:545–558.
3. Stys PK, Zamponi GW, van Minnen J, Geurts JJG (2012) Will the real multiple sclerosis please stand up? *Nat Rev Neurosci* 13:507–514.
4. Wijnands JMA, et al. (2017) Health-care use before a first demyelinating event suggestive of a multiple sclerosis prodrome: A matched cohort study. *Lancet Neurol* 16:445–451.
5. Xia Z, et al. (2017) Assessment of early evidence of multiple sclerosis in a prospective study of asymptomatic high-risk family members. *JAMA Neurol* 74:293–300.
6. Musse AA, Boggs JM, Harauz G (2006) Deimination of membrane-bound myelin basic protein in multiple sclerosis exposes an immunodominant epitope. *Proc Natl Acad Sci USA* 103:4422–4427.
7. Wood DD, Bilbao JM, O'Connors P, Moscarello MA (1996) Acute multiple sclerosis (Marburg type) is associated with developmentally immature myelin basic protein. *Ann Neurol* 40:18–24.
8. Bradford CM, et al. (2014) Localisation of citrullinated proteins in normal appearing white matter and lesions in the central nervous system in multiple sclerosis. *J Neuroimmunol* 273:85–95.
9. Moscarello MA, Wood DD, Ackerley C, Boulias C (1994) Myelin in multiple sclerosis is developmentally immature. *J Clin Invest* 94:146–154.
10. Weil M-T, et al. (2016) Loss of myelin basic protein function triggers myelin breakdown in models of demyelinating diseases. *Cell Rep* 16:314–322.
11. Shaharabani R, et al. (2016) Structural transition in myelin membrane as initiator of multiple sclerosis. *J Am Chem Soc* 138:12159–12165.
12. Barnett MH, Prineas JW (2004) Relapsing and remitting multiple sclerosis: Pathology of the newly forming lesion. *Ann Neurol* 55:458–468.
13. Lucchinetti C, et al. (1999) A quantitative analysis of oligodendrocytes in multiple sclerosis lesions. A study of 113 cases. *Brain* 122:2279–2295.
14. Locatelli G, et al. (2012) Primary oligodendrocyte death does not elicit anti-CNS immunity. *Nat Neurosci* 15:543–550.
15. Traka M, Podojil JR, McCarthy DP, Miller SD, Popko B (2015) Oligodendrocyte death results in immune-mediated CNS demyelination. *Nat Neurosci* 19:65–74.
16. Scheld M, et al. (2016) Neurodegeneration triggers peripheral immune cell recruitment into the forebrain. *J Neurosci* 36:1410–1415.
17. Baxi EG, et al. (2015) Transfer of myelin-reactive th17 cells impairs endogenous remyelination in the central nervous system of cuprizone-fed mice. *J Neurosci* 35:8626–8639.
18. Steinman L, Shoenfeld Y (2014) From defining antigens to new therapies in multiple sclerosis: Honoring the contributions of Ruth Arnon and Michael Sela. *J Autoimmun* 54:1–7.
19. Ludwin SK (1978) Central nervous system demyelination and remyelination in the mouse: An ultrastructural study of cuprizone toxicity. *Lab Invest* 39:597–612.
20. Emerson MR, Biswas S, LeVine SM (2001) Cuprizone and piperonyl butoxide, proposed inhibitors of T-cell function, attenuate experimental allergic encephalomyelitis in SJL mice. *J Neuroimmunol* 119:205–213.
21. Herder V, et al. (2012) Cuprizone inhibits demyelinating leukomyelitis by reducing immune responses without virus exacerbation in an infectious model of multiple sclerosis. *J Neuroimmunol* 244:84–93.
22. Hillis JM, Davies J, Mundim MV, Al-Dalahmah O, Szele FG (2016) Cuprizone demyelination induces a unique inflammatory response in the subventricular zone. *J Neuroinflammation* 13:190.
23. Harauz G, Musse AA (2007) A tale of two citrullines–Structural and functional aspects of myelin basic protein deimination in health and disease. *Neurochem Res* 32:137–158.
24. Tejeda EJC, et al. (2017) Noncovalent protein arginine deiminase (PAD) inhibitors are efficacious in animal models of multiple sclerosis. *J Med Chem* 60:8876–8887.
25. Norton WT, Poduslo SE (1973) Myelination in rat brain: Method of myelin isolation. *J Neurochem* 21:749–757.
26. Sawcer S, et al.; International Multiple Sclerosis Genetics Consortium; Wellcome Trust Case Control Consortium 2 (2011) Genetic risk and a primary role for cell-mediated immune mechanisms in multiple sclerosis. *Nature* 476:214–219.
27. Xia Z, et al. (2016) Genes and Environment in multiple sclerosis project: A platform to investigate multiple sclerosis risk. *Ann Neurol* 79:178–189.
28. Giovannoni G (2017) The neurodegenerative prodrome in multiple sclerosis. *Lancet Neurol* 16:413–414.
29. Bove RM, Hauser SL (2018) Diagnosing multiple sclerosis: Art and science. *Lancet Neurol* 17:109–111.
30. Dhaunchak AS, et al.; Canadian Pediatric Demyelinating Disease Group (2012) Implication of perturbed axoglial apparatus in early pediatric multiple sclerosis. *Ann Neurol* 71:601–613.
31. Itoyama Y, et al. (1980) Immunocytochemical observations on the distribution of myelin-associated glycoprotein and myelin basic protein in multiple sclerosis lesions. *Ann Neurol* 7:167–177.
32. Rodriguez M, Scheithauer B (1994) Ultrastructure of multiple sclerosis. *Ultrastruct Pathol* 18:3–13.
33. Aboul-Enein F, et al. (2003) Preferential loss of myelin-associated glycoprotein reflects hypoxia-like white matter damage in stroke and inflammatory brain diseases. *J Neuropathol Exp Neurol* 62:25–33.
34. Ludwin SK, Johnson ES (1981) Evidence for a "dying-back" gliopathy in demyelinating disease. *Ann Neurol* 9:301–305.
35. Cao L, Goodin R, Wood D, Moscarello MA, Whitaker JN (1999) Rapid release and unusual stability of immunodominant peptide 45-89 from citrullinated myelin basic protein. *Biochemistry* 38:6157–6163.
36. Raijmakers R, et al. (2005) Citrullination of central nervous system proteins during the development of experimental autoimmune encephalomyelitis. *J Comp Neurol* 486:243–253.
37. Moscarello MA, et al. (2013) Inhibition of peptidyl-arginine deiminases reverses protein-hypercitrullination and disease in mouse models of multiple sclerosis. *Dis Model Mech* 6:467–478.

IMMUNOLOGY AND INFLAMMATION